

1

2   **Automated surface feature selection using SALSA2D: An**  
3   **illustration using Elephant Mortality data in Etosha National Park**

4   L.A.S Scott-Hayward<sup>a</sup>, M.L. Mackenzie<sup>a</sup>, C.G. Walker<sup>b</sup>, G. Shatumbu<sup>c</sup>, W. Kilian<sup>c</sup>  
5   and P. du Preez<sup>d</sup>

6   <sup>a</sup>School of Mathematics and Statistics, University of St Andrews, KY16 9LZ, Fife, Scotland;

7   <sup>b</sup>Department of Engineering Science, University of Auckland, 70 Symonds Street, Auckland,

8   New Zealand; <sup>c</sup>Etosha Ecological Institute, PO Box 6, Okaukuejo via Outjo, Ministry of

9   Environment, Forestry and Tourism, Namibia; <sup>d</sup>African Wildlife Conservation Trust, PO

10   box 97401, Windhoek, Namibia

11   <sup>a</sup>ORCID: LSH (0000-0003-3402-533X), MLM (0000-0002-8505-6585)

12   **ARTICLE HISTORY**

13    Compiled June 24, 2022

14   **Open Research Statement**

15   The data and code are provided as private-for-peer review but can be made pub-

16   lic if accepted for publication. The files can be found at the github site of the

17   first/corresponding author: <https://github.com/lindesaysh/MIKE>. Addition-

18   ally, the data file will be made public and permanently archived in the St Andrews

19   PURE repository.

## ABSTRACT

This analysis is motivated by the MIKE dataset in Etosha National Park (ENP).

We use this dataset to show the development of an automated selection method for regression models to replace the model averaging used in the original CReSS paper. This method shows clear numerical and practical benefits over model averaging, and its application to the elephant carcass data are of immediate and practical value to a range of stakeholders.

We have developed SALSA 2D in a GLM/GAM regression framework but this paper shows the flexibility of this approach by applying it to presence only data and use a downweighted Poisson regression. Using SALSA2D for model selection provided a more realistic local/clustered intensity surface compared with the model average approach.

The full analysis results showed high carcass intensity close to water holes and roads and in areas of the park with average rainfall. Some high risk areas were identified and these revelations are important for effective park management, particularly mitigation of poaching. It is impossible to patrol such a large area at random and these high intensity areas (particularly those accessed by a subset of roads and near some waterholes) can be targeted for more monitoring efforts than others.

## KEYWORDS

CReSS (Complex Region Spatial Smoother); Spatially Adaptive; SALSA; spline; point process; GLM

## 1. Introduction

### 1.1. *Motivating Example*

The Monitoring the Illegal Killing of Elephants (MIKE; <https://cites.org/eng/prog/mike/index.php/portal>) programme is an international collaboration that collects and monitors trends related to the illegal killing of Elephants from across Africa and Asia [1]. The MIKE project also seeks to monitor the effectiveness of field conservation efforts and is part of the Convention on International Trade in Endangered Species of Wild Fauna and Flora (CITES) initiative. MIKE operates in over 80 sites, across 43 elephant range states across Africa and Asia and rigorous protocols have been developed as part of this initiative to collect, analyse and

52 build the capacity to better enforce the law and to reduce illegal elephant killings.  
 53 The overall goal of MIKE is to provide information needed for elephant range states  
 54 to make appropriate management and enforcement decisions, and to build institu-  
 55 tional capacity within the range states for the long-term management of their ele-  
 56 phant populations. In particular, they report PIKE (Proportion of Illegally Killed  
 57 Elephants) for every range state.  
 58 The MIKE project has been active in Etosha National Park (ENP) in Namibia for  
 59 over a decade, and substantial resources are used to collect relevant abundance and  
 60 mortality data by dedicated aerial surveys under strict survey protocols. As part of  
 61 routine park activities, opportunistic data also contributes to the African Elephant  
 62 (*Loxodonta africana*) mortality database.  
 63 To meet the needs of the MIKE project and more generally, there is an urgent  
 64 need to understand both the magnitude and spatial patterns of elephant deaths in  
 65 ENP, regardless of cause. If the deaths are natural and, for instance, disease-related  
 66 (e.g. anthrax) then this provides valuable information about the prevalence and lo-  
 67 cale of disease in the park. Endemic anthrax occurs in Etosha annually [2] and plays  
 68 an important role in elephant population regulation/limitation. The monitoring of  
 69 the prevalence of anthrax in elephant is important, because it advances our knowl-  
 70 edge of a top down factor limiting a mega-herbivore. If instead, the deaths are a  
 71 result of poaching then this provides necessary information about the prevalence,  
 72 locale and patterns of these deaths.  
 73 Whilst in 2018 the poaching of elephants in ENP was low (20 deaths reported to  
 74 MIKE and none poached), the general trend in more recent years is increasing (*pers.*  
 75 *comm.* Etosha Ecological Institute). As the number of poached elephants increases  
 76 it is very useful knowledge to have a baseline distribution of natural deaths. The de-  
 77 velopment of statistical modelling methods aimed at predicting elephant mortality  
 78 risk is crucial for early carcass detection. Should poaching occur in regions not com-  
 79 mon to find natural deaths, then increased/targeted mitigation measures can be effi-  
 80 ciently actioned. Practically, understanding both the magnitude and spatial patterns  
 81 of elephant deaths in ENP may assist in adapting patrol efforts in and around the

82 park to track the anthrax disease and/or combat any poaching activities. It is also  
 83 very important in light of the mass death events seen in Botswana in 2020 and 2021  
 84 [3]. Having a sense of “normal“ places of natural death may provide insights should  
 85 such events ever occur in Etosha.

86 Statistical modelling of these data is necessary since the park is very large ( $\sim 23,000$   
 87  $\text{km}^2$ ) and regardless of the survey regime, the observed counts will undoubtedly  
 88 comprise a subset of a larger number of deaths. Reliable modelling results which  
 89 accurately estimate the magnitude and location of elephant mortality in ENP are  
 90 also not guaranteed and require the careful consideration of at least the following  
 91 two points, 1) most wildlife, including elephant, rarely traverse a large salt pan:  
 92 there is little vegetation to be found in the pan and the sometimes boggy terrain  
 93 prevents travel for large animals such as elephant; 2) the spatial patterns of mortal-  
 94 ity are likely to be localised and patchy: the abundance of elephant in the park is far  
 95 from homogeneous and the reasons for death (natural or otherwise) are also likely to  
 96 vary across the park. Failing to account for the possibly unusual spatial patterns in  
 97 these data and/or assuming points across the pan are as closely linked as equidistant  
 98 points without a physical barrier, can unwittingly lead to false conclusions about the  
 99 magnitude and location of elephant deaths in the park.

100 The Complex Region Spatial Smoother (CReSS) is a regression spline based sta-  
 101 tistical modelling method equipped to address both aspects of these data [4]. Eu-  
 102 clidean or geodesic (‘around the salt pan’) distances can be used to underpin the  
 103 smoothed surface and the method is spatially adaptive enabling the targeting of sur-  
 104 face flexibility to accommodate any particularly patchy trends and/or local surface  
 105 features. While appropriate, the currently published CReSS method [4] undertakes  
 106 the, crucially important, model selection process using a model-averaging of predic-  
 107 tions approach which can be computationally intensive. We have also found after  
 108 extensive use that this can mask unusually shaped spatial patterns when these are  
 109 observed. In this paper, we propose using CReSS with an automated model selec-  
 110 tion approach, as an alternative to model-averaging, which enables atypical spatial  
 111 patterns to be deduced from the data - patterns which have implications for park

management in this case, and produces one model which is easier to handle.

## 1.2. Statistical development

The statistical development here involves the creation of a conceptually simple but effective heuristic algorithmic approach to carry out model selection for multidimensional basis functions to determine overall surface flexibility (via the number of ‘knots’) and the targeting of this flexibility (via ‘knot’ locations). The development of this algorithm was based on the Spatially Adaptive Local Smoothing Algorithm (SALSA) [5], which is for univariate smoothing. In order to distinguish the new algorithm, it will be referred to in this paper as SALSA2D.

We have also extended the suite of CReSS basis functions that can be used for the two-dimensional smoothing. This is useful since SALSA2D is agnostic about the basis function used but relies instead on an objective fit criteria for execution.

The new basis and SALSA2D algorithm are all implemented inside the `MRSea` R package [6, 7] for easy use by practitioners.

## 2. Methodology

### 2.1. The Complex Region Spatial Smoother(CReSS)

The published CReSS approach [4] achieves spatially adaptive surfaces via a judicious weighting of a variety of candidate surfaces with ‘space-filled’ knots [8] ranging from the very simplistic (via small numbers of knots with basis functions with a relatively global influence) to very complex (via large numbers of knots with basis functions with a relatively localised influence). This approach has also shown to perform well against other model-based alternatives developed for data sets with internal exclusion zones (such as coastlines and island systems) and is finding use in a range of ecological applications [9–11].

The CReSS approach fits pure spatial regression models to a set of coordinates  $\mathbf{x}$  of the form:

$$g(\mathbf{y}) = \eta = \beta_0 + s(\mathbf{x}) \quad (1)$$

where  $g$  is the link function and  $\eta$  the linear predictor.  $\mathbf{s}$  is a two dimensional surface approximated by a linear combination of exponential basis functions  $bE$ .

$$bE_{ki} = \exp(-h_{ki}/r_k^2) \quad (2)$$

where  $r_k$  dictates the extent of the decay of this exponential function with distance between points, and thus the extent of its local nature. Notably  $h_{ki}$  indicates a geodesic or Euclidean distance (for some observation  $i$  and the  $k$ -th knot location). Parameter  $r_k$  takes values such that if  $r_k$  is small the model will have a set of relatively local basis functions and if  $r_k$  is large the model will have a set of relatively global basis functions. The exact values of  $r_k$  are dependent upon the range and units of the spatial covariates.

After the choice of distance metric, the CReSS with model averaging procedure fits multiple models with each model evaluated at one of a variety of parameter values for the number of knots ( $K$ ) and the effective range parameter ( $r$ ). According to Scott-Hayward et al. [4] model selection is achieved using  $AIC_c$  [12] weights and averaging those models with  $\Delta AIC_c < 10$  to produce weighted predictions.

While this approach (CReSS with model averaging) has been shown to produce reliable results in many cases [4], this procedure can be complicated, in terms of model handling and difficult to assess model fit and to provide confidence intervals. A paper by Dormann et al. [13] highlights some of the limitations of a model averaging approach. Namely, the authors show that estimating model weights introduces unknown and unaccounted for uncertainty and that confidence intervals for model-averaged predictions rarely achieve nominal coverage. They also state that model averaging is most useful when the predictive error of contributing model predictions

160 is dominated by variance (as opposed to bias), and if the covariance between mod-  
 161 els is low. We argue that ecological data, including the carcass data seen here, is  
 162 often highly variable with limited covariates and thus could result in prediction er-  
 163 rors dominated by variance. Additionally, given the CReSS with model averaging  
 164 approach averages models with the same covariates but different parameterisations,  
 165 there is also likely to be high covariance between competing models, rendering the  
 166 model averaging approach less appropriate.

167 Further, when the spatial patterns are particularly unusual (e.g. stripe-like features  
 168 or local hotspots are genuinely present) we have found that a model-averaging ap-  
 169 proach can result in overly smooth surfaces which mask these unusual, but impor-  
 170 tant, patterns. This may result for a variety of reasons: under the original CReSS  
 171 approach the space-filled knots are fixed in position for a given knot number, and  
 172 the extent that each basis function is local (or global) is fixed (and the same) for all  
 173 knots in that candidate surface.

174 As part of recent work, we have expanded the CReSS approach to include a Gaus-  
 175 sian radial basis to the choice of basis functions available for selection. The two  
 176 bases have different shapes, with the exponential being more peaked at the centre.  
 177 These choices allow for more nuanced model fitting, akin to link function or distance  
 178 metric choice. The Gaussian radial basis,  $bG$ , is specified as:

$$bG_{ki} = \exp^{-(h_{ki}r_k)^2} \quad (3)$$

179 where  $r_k$  and  $h_{ki}$  are as defined for the exponential (Equation 2) except that for the  
 180 Gaussian basis, a small value for  $r_k$  returns a relatively global basis and a large  $r_k$   
 181 value returns a relatively local basis.

## 2.2. Spatially Adaptive Local Smoothing Algorithm for at least two dimensions (SALSA2D)

SALSA2D uses the same model framework as for model averaging (see Equation 1) but where  $k$  is chosen using an iterative three step procedure. The algorithm works in (at least) two dimensions and begins with space-filled knots to facilitate spatial coverage and then adaptively moves, adds and drops knots into, or from, locations in line with poor model fit (evidenced by large residuals) and an objective fit criteria. At each stage, the global/local extent of each basis function via the  $r_k$  value employed can also be revised as part of the search for a more appropriate surface. So, unlike the model averaging approach, SALSA2D returns one model with specifically selected  $k$  and  $r_k$  enabling standard methods for assessment of fit and uncertainty estimation.

The algorithm that drives SALSA2D has an iterative 3-step structure. After an initialisation step, there are three repeated steps: the first is a simplification step to reduce the number of estimated parameters which is achieved by allowing for the removal of columns from the design matrix (reduction in knot number). The second and third steps (exchange and improve) are designed to efficiently search the model space (all possible number and locations of knots). The exchange step allows for the possibility of moving away from a local optimum or addition of columns to the design matrix (a new knot) and the improvement step attempts to make local improvements in knot location. The outcome of each of these steps is determined by an objective fit criterion and repeated until no improvements are made (or an iteration limit is reached). The structure of the algorithm is given in the pseudo code in Figure 2.2 and the next sections describe the steps in detail.

### 2.2.1. Initialisation

Each observed location,  $i$ , is considered a possible location for a knot position. To avoid estimation issues, only unique knot locations are considered giving  $K_l$  legal knot locations. The user specifies a starting number of knots,  $K_s$ , where  $K_s < K_l$ , and these are selected from  $K_l$  using a space-filling algorithm [8]. This method pro-



```

SALSA2D:
Given an  $n$ -dimensional set  $K_l$  of possible knot locations over the region of interest.
  Initialise
    Initialise knots,  $K_s$  within the points of  $K_l$ 
    Check for convergence
  Repeat
    Repeat Simplification step while ( $K > K_{\min}$  and fit measure improves)
    Repeat Exchange step while ( $K < K_{\max}$  and fit measure improves)
    Repeat Improvement step while (fit measure improves)
  While (an improvement in fit measure is made by one of the above steps)

```

**Figure 1.** Pseudo-code outlining the structure of SALSA2D [adapted from Figure 1, 5], where  $K$  is the number of knots used for fitting.

vides good coverage across the spatial region as a starting position for SALSA2D. Additionally, the minimum number of knots,  $K_{\min}$  ( $2 \leq K_{\min} < K_s$ ) and maximum number  $K_{\max}$  ( $K_s < K_{\max} \leq K_l$ ) are specified. To evaluate the basis function, the  $r_k$ -value for each basis must also be chosen. The SALSA2D algorithm selects from  $R$  possible options for  $r_k$  which range from a very local basis to a globally acting basis. The middle option which is neither very local or very global, is chosen to initialise the first model. To ensure that the initial model fit has converged, there is a drop step component that is activated if the variance of the initialised first model exceeds that of the simpler input model (the variance should not increase with additional parameters/flexibility in the model). If this occurs, knot locations with the largest contributions to the variance are removed one by one until the overall variance of the more complex model is lower than the input model.

### 2.2.2. The simplify step

Using the fit criteria specified, the simplify step compares the current model with all models obtained by removing an existing knot (as long as this is at least  $K_{\min}$ ). At each iteration, the model with the best fitness measure is retained and the process repeated until there is no further improvement in the fitness measure. This step can be carried out by fixing  $r_k$  or by choosing  $r_k$  for each basis as each knot is dropped

230 for comparison.

### 231 2.2.3. *The exchange step*

232 The exchange step increases the extent of the search of model space by enabling a  
233 move away from a local minima (of the fit criterion). It uses the maximum Pearson  
234 residual from the current fitted model to identify a possible candidate location for  
235 a new knot (although in theory other types of residuals could be chosen and we use  
236 an alternative metric for the point process models in the next sections). The algo-  
237 rithm then compares the objective fit criteria for these models that result when each  
238 of the existing knots in the current model is moved to this new location, and also  
239 the fit criteria from the model that results when an additional knot at this location  
240 is added to the current model (if this does not exceed  $K_{\max}$ ). The model with the  
241 best fitness measure is retained in this step if it has a better fitness measure than  
242 the current model. Evaluation of each of these models can be very quick to return  
243 but this process is naturally more computationally expensive, if  $r_k$  is also chosen  
244 for each basis function for each candidate model. In practice, the algorithm uses the  
245 knot locations of the five largest residuals as candidates for an exchange or move.

### 246 2.2.4. *The improve step*

247 The improve steps allows a more nuanced search of the local minima by allowing  
248 small adjustments to the location of each knot. Using the fit criteria specified, the  
249 improve step compares the current model with all models obtained by moving an ex-  
250 isting knot to one of its five nearest neighbours (determined by the distance metric  
251 employed: geodesic or Euclidean). At each iteration, the model with the best fitness  
252 measure is retained. As with the exchange step, alternative choices for the  $r_k$  param-  
253 eter may be considered when fitting each new model and this process is likely to be  
254 swift at this stage.

### 255 2.2.5. Determining $r_k$

256 This routine considers incrementing or decrementing  $r_k$  values in the sequence of  
257  $R$  possible values, where the sequence is selected using the method from 4. It can  
258 be evaluated either once at the end of the exchange, improve and simplify steps or  
259 as part of every decision taken during these steps. The process is done by consid-  
260 ering each of the radial basis columns in turn, and incrementing or decrementing  
261 the  $r_k$  values in the index until there is no improvement in the fitness measure. At  
262 each step the  $r_k$ -values for the other basis columns are maintained at the current  
263 solution. The best of these models is selected as the new current model, and the  
264 process iterates until no improvement is made. This process can have a large com-  
265 putational overhead and may significantly prolong the procedure but constitutes a  
266 broader search of the model space.  
267 This algorithm is implemented in the MRSea package which can be found at [www.](http://www.github.com/lindesaysh/MRSea)  
268 [github.com/lindesaysh/MRSea](http://github.com/lindesaysh/MRSea) [6].

## 269 3. Methods comparison

270 This section compares the performance of the CReSS with model-averaging ap-  
271 proach to CReSS with SALSA2D for model selection. The methods are compared  
272 numerically using log-likelihood, while the practical consequences of using each are  
273 assessed visually and contextualised using surface features in Etosha National Park,  
274 Namibia.

### 275 3.1. Data specification

276 To appreciate the numerical and practical benefits of this methodological develop-  
277 ment, the MIKE data was used for the method comparison and for the subsequent  
278 analysis in full [1]. These data consists of 320 carcass locations observed between  
279 February 2000 and March 2017 in Etosha National Park (ENP). The observed fa-  
280 talities are recorded as being due to: anthrax, natural (age-related) causes, poach-  
281 ing and unknown. While a substantial proportion of the carcasses are recorded as

282 being for ‘unknown’ reasons (54%) the largest known cause of death is from An-  
 283 thrax (27.8%). Less than 1% of the carcasses were confirmed as poached. Disregard-  
 284 ing 2017 as it was only a partial year, 2006, 2013 and 2014 had the fewest recorded  
 285 carcasses (7-8), whilst 2002, 2003, 2005 and 2011 had the highest recorded (27-28).  
 286 As there were a relatively small number of observations per year, no guarantee the  
 287 deaths occurred in the year of detection and no obvious changes in the spatial pat-  
 288 tern of observations, the data were pooled across years.  
 289 The longitude and latitude coordinates were converted to Universal Transverse Mer-  
 290 cator (UTM) zone 33S and the study region was extended beyond the ENP bound-  
 291 ary by 20 km to allow for the inclusion of carcasses just outside the park. Addition-  
 292 ally, the large salt pan was reduced in size by 2 km to allow inclusion of carcasses  
 293 found near the edge of the pan. The data show that carcasses generally seem to oc-  
 294 cur near roads (or, at least, are more commonly observed near roads) and water-  
 295 holes (Figure 2). It is possible that these patterns are due to opportunistic reporting  
 296 of carcasses as a result of park vehicles moving along the roads, however the data  
 297 were from both opportunistic and dedicated surveys, which are carried out with-  
 298 out reference to roads. Furthermore, collared elephant in ENP have been shown to  
 299 utilise roads/tracks and fire breaks extensively and are known to frequent waterholes  
 300 [14].

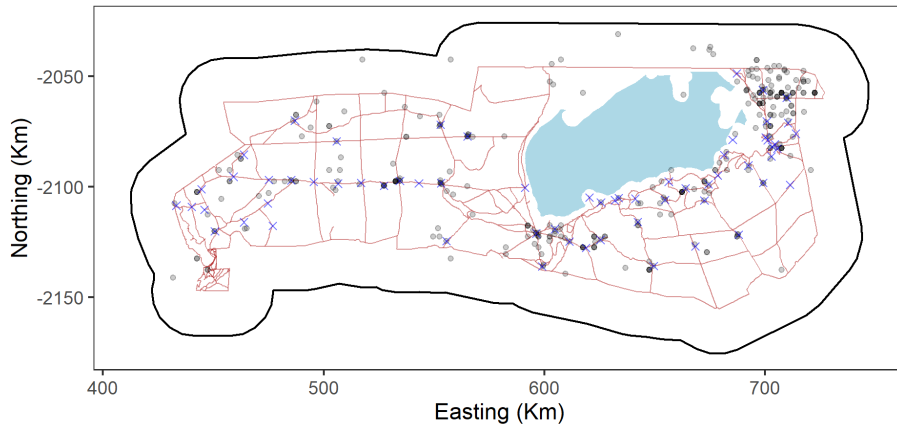


**Figure 2.** Figure showing the study area (ENP) with the carcass locations shown as dots. As there are duplicate locations, the darker the dot, the more presence locations. The study area (park boundary plus 20km buffer) is outlined in black. The blue polygon is the Etosha salt pan, the red lines are park roads and the blue crosses are waterholes. The outermost red line is also the park fence.

301 In much of the grey literature the methods described here have been applied in a  
 302 Poisson or Binomial generalised additive model framework (GAM). Here we have  
 303 chosen to showcase the versatility of the SALSA algorithms and apply them to a  
 304 presence only data set, where the primary interest are the spatial locations of pres-  
 305 ence points (carcass locations). In this data set, the link back to the original survey  
 306 effort (where surveys were undertaken) is not available so we are left with only the  
 307 carcass locations and no absence locations. Warton and Shepherd [15] showed the  
 308 link between logistic regression and an inhomogeneous Poisson point process model  
 309 (PPM) and here we use both this link and the downweighted Poisson regression  
 310 method [16] to fit a Poisson PPM using a pure regression GAM framework. In this  
 311 case, the intensity is the number of presence records (carcass sightings) per unit area  
 312 and is modelled as a function of covariates measured throughout the study region.  
 313 It is a relative measure and gives the expected abundance of carcass sightings for a  
 314 given area.

315 Pseudo-absences in the regression setting play the same role as quadrature points  
 316 in point process modelling and we used the point process framework to choose the  
 317 number and location of these points. The pseudo-absence points were selected as a  
 318 regular grid and the number based on convergence of the likelihood [16].

319 Lastly, to determine areas of poor fit, the exchange step requires the calculation of  
 320 residuals. This was achieved by creating a neighbourhood around each knot location  
 321 ( $k$ ) and comparing the observed number of points with the sum of the estimated  
 322 intensities in the same area. For more details, see Section 1 of the Supplementary  
 323 Material.

### 324 3.2. Model specification

325 To compare the performance of SALSA2D with model averaging as a model selec-  
 326 tion approach, models with a two dimensional smoother-based term for geographic  
 327 locations were fitted to the MIKE data. The comparison involved either the pub-  
 328 lished CReSS method which employs model averaging [4] or model selection using  
 329 SALSA2D to determine knot number and location. Here we model the the loca-  
 330 tions of the carcasses jointly with the pseudo-absences by maximising the following  
 331 weighted Poisson log-pseudolikelihood [17]:

$$l(\beta; \mathbf{X}) = \sum_{i=1}^N w_i (y_i \log(\lambda(\mathbf{X}_i)) - \lambda(\mathbf{X}_i)) \quad (4)$$

332 where  $\lambda(\mathbf{X}_i)$  is the intensity at location  $i$ ,  $\mathbf{X}_i$  represents the design matrix at lo-  
 333 cation  $i$ ,  $N$  is the total number of points (presence and pseudo-absence),  $\mathbf{w} =$   
 334  $\{w_1, \dots, w_N\}$  are quadrature weights.

$$y_i = \begin{cases} \frac{1}{w_i} & \text{if } i \text{ is a presence location} \\ 0 & \text{if } i \text{ is a pseudo-absence location} \end{cases}$$

335 The log-pseudolikelihood in Equation 4 [17] is a re-expression of the Poisson PPM  
 336 log-likelihood [18], which means that models can be fitted using standard GLM soft-  
 337 ware. Here we model the expected number of carcasses per square kilometre and  
 338 so the weights for the pseudo-absence points are specified as the area of the study  
 339 region, 37,872 km<sup>2</sup> (ENP plus the 20 km buffer) divided by the number of pseudo-  
 340 absences. The weights for presence points are set to some small value ( $10^{-6}$ ).  
 341 Likelihood convergence was used to determine the the number of pseudo-absences  
 342 which was estimated to be 9644 (a grid spacing of 2 km). For more details see Sec-  
 343 tion 2 of the Supplementary Material.  
 344 For this method comparison section, we model the intensity as a function of coordi-

345 nates,  $\mathbf{x}$ , only.

$$\log(\lambda(\mathbf{X}_i)) = \eta_i = \beta_0 + s(\mathbf{x}) = \mathbf{X}_i^T \boldsymbol{\beta} \quad (5)$$

346 where  $\eta_i$  is the linear predictor, consisting of the intercept,  $\beta_0$ , and a smooth func-  
 347 tion of coordinates,  $s(\mathbf{x})$ . The smooth function is either the exponential or Gaussian  
 348 basis function.

349 For both the model averaging and SALSA2D methods, the following specifications  
 350 were used to return the columns of the design matrix  $\mathbf{X}$  in Equation 5:

- 351 • Two basis options: Exponential ( $bE_{ki}$ ; Equation 2) or Gaussian ( $bG_{ki}$ ; Equa-  
 352 tion 3)
- 353 • Two distance measures (Euclidean or geodesic) to calculate  $h$  in the basis  
 354 equations; the geodesic distances are calculated using Floyds algorithm [19]  
 355 and for more details see [4].
- 356 • 12 choices of fixed knot number (for the model-averaging approach) and 12  
 357 choices of starting knot numbers,  $K_s$  for the SALSA2D approach. In each  
 358 case, the fixed/starting knot set was: [5, 10, 15, ..., 55, 60]. A total of 285 le-  
 359 gal knot positions ( $K_l$ ) were considered. These consisted of all non-duplicated  
 360 carcass locations (n=245) and 50 space-filled pseudo-absence locations ( $\sim 20\%$   
 361 of all  $K_l$ ).
- 362 • 10 choices of  $r_k$  (also specified as part of Equations 2 and 3)

363 Additionally, for SALSA2D,  $K_{\min}$  and  $K_{\max}$  were set to 2 and 100 respectively, for  
 364 all model specifications.

### 365 **3.3. Model comparison**

366 In keeping with Scott-Hayward et al. [6], the model-averaging CReSS method was  
 367 governed by  $AIC_c$  weights which were used to choose which models to average  
 368 ( $\Delta AIC_c \leq 10$ ) and their relative contribution to the overall averaged model. In

keeping with Walker et al. [5], the BIC was used to govern SALSA2D model selection regarding the choice of knot number and their locations across the range of combinations of basis type, distance metric, starting knot number and  $r_k$  choices [20]. In all cases, the log-likelihood score (Equation 4) was calculated for each model to enable comparison between model selection strategies.

## 4. Results

### 4.1. Numerical comparison

The log-likelihood scores returned for the model averaging method were fairly close (maximum difference 14 points) regardless of the basis function and distance metric used in each model (Table 1, Method: ‘Model averaging’). The geodesic-exponential combination scored the best (largest log-likelihood) of the 4 combinations trialled. Interestingly, this combination chose 11 models with which to average over to obtain this solution, compared with some options that chose far fewer models to use as part of the average calculation. In general, geodesic distances were preferred to Euclidean regardless of basis.

**Table 1.** Table showing the results of the model averaging and SALSA2D methods of model selection for a given basis type and distance metric used. The ‘No. Models’ indicates the number of models chosen to carry out the model averaging in each case, and the ‘No. Knots’ indicates the number of knots chosen for each model using the SALSA2D selection method. The star indicates the model with the largest log-likelihood (LL) score, and thus the chosen model based on the LL in each case.

Method	Basis	Distance Measure	No. Models	No. Knots	Log-Likelihood
MA	Exponential*	Geodesic	11	-	-1432.0
	Gaussian	Geodesic	2	-	-1441.5
	Exponential	Euclidean	1	-	-1443.4
	Gaussian	Euclidean	8	-	-1446.3
SALSA2D	Exponential	Geodesic	-	32	-1369.7
	Gaussian	Geodesic	-	32	-1408.3
	Exponential*	Euclidean	-	41	-1301.6
	Gaussian	Euclidean	-	47	-1541.6

The log-likelihood scores for the SALSA2D based selection are shown for the model with the highest log-likelihood for each of the basis/distance metric combinations



386 (Table 1, Method: SALSA2D). Across the four combinations, the scores were less  
 387 homogeneous than for the model averaging results and the exponential-Euclidean  
 388 SALSA2D model (using 41 knots) was the best of all trialled here. In contrast to the  
 389 averaging approach, there was a preference for the exponential basis with the dis-  
 390 tance metric secondary. In reality, the user may prefer to select the best model using  
 391 BIC (as was used for  $k/r$  selection). In this case, the order of the four parameteri-  
 392 sations was the same (exponential-Euclidean the best and Gaussian-Euclidean the  
 393 worst) and the best model using BIC was the same as in Table 1 when log-likelihood  
 394 was used (see Section 3 of the supplementary material for an expanded version of  
 395 Table 1).

396 Using the “best” SALSA2D models only, for all but one combination of basis type  
 397 and distance metric used, all SALSA2D models produced better scores than the  
 398 model averaging method – sometimes reducing the log-likelihood score by as much  
 399 as 10%. However, if SALSA2D initialises with too few knots, the algorithm may get  
 400 stuck in local minima. So long as a large enough number of starting knot locations  
 401 was selected ( $\sim \geq 40$ ), SALSA2D-based selection resulted in superior scores over  
 402 the model-averaging alternative (Figure 3). This demonstrates that the SALSA2D  
 403 model selection method can return improved results and at worst, SALSA2D results  
 404 were almost indistinguishable from the best model averaging-based result.

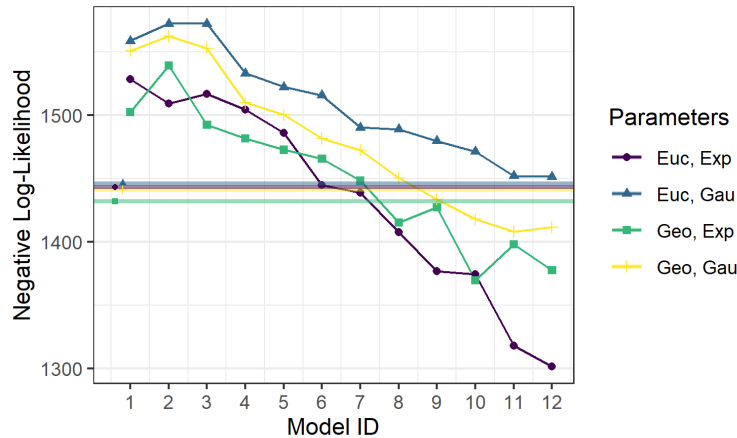


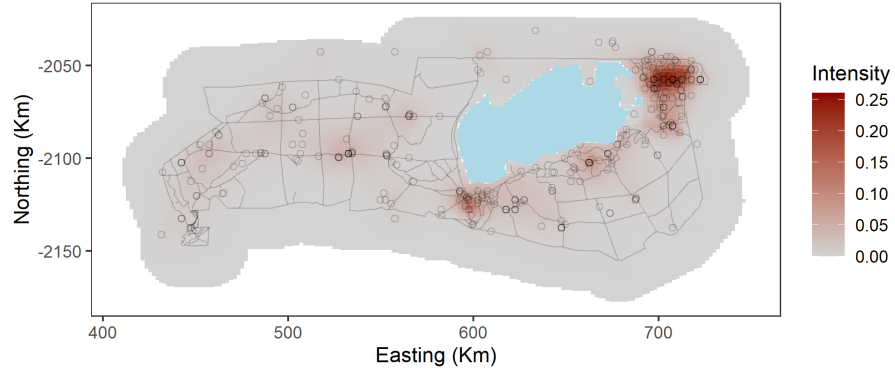
**Figure 3.** Figure showing the model identification number (increasing start knots) and the negative log-likelihood score for each of the SALSA2D models resulting from a different start knot number,  $K_s$ . The horizontal lines are the scores for the equivalent model averaging result.

## 405 4.2. Visual comparison

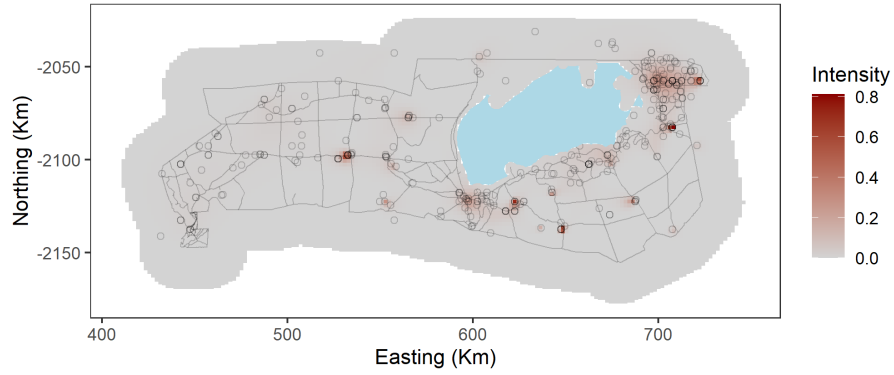
406 Results for the model-averaging based model (Figure 4a) signalled that the inten-  
407 sity of carcasses was highest in the north-east of the park (where most the observed  
408 deaths occurred) and along the southern edge of the large salt pan, which is consis-  
409 tent with the observed data. The carcass intensity is very low near the south-west  
410 and South-Eastern borders of ENP.

411 Whilst the model averaging results show a smooth intensity surface, the SALSA2D  
412 method produces a more clustered intensity surface (Figure 4b). The surface shows  
413 more local effects, particularly the centre west and below the salt pan and the high-  
414 est intensity at these spots was nearly three times that of the model-averaging re-  
415 sult. These effects, match well with the carcass location data and frequently occur at  
416 the confluence of several roads and some waterholes.

417 Figure 5 shows the selected knot locations and equivalent  $r$  parameter from the 11  
418 averaged models (Figure 5a) and the one best SALSA2D model (Figure 5b). The  
419 averaged knot locations are more difficult to represent but it can be seen that there  
420 are multiple  $r$  values (ranging from global to very local) across the same locations  
421 and occasionally a location where the sign of the coefficient changes between mod-  
422 els. The SALSA2D result is more nuanced with very few knot locations selected to  
423 the west of the park. For the 41 selected locations, a variety of  $r$ 's were chosen. It is  
424 interesting that the SALSA2D approach found the Euclidean distance metric to be  
425 best and it is possible that the more local knots chosen under this method negate  
426 the need for the geodesic distances by limiting the possible leakage across the pan.

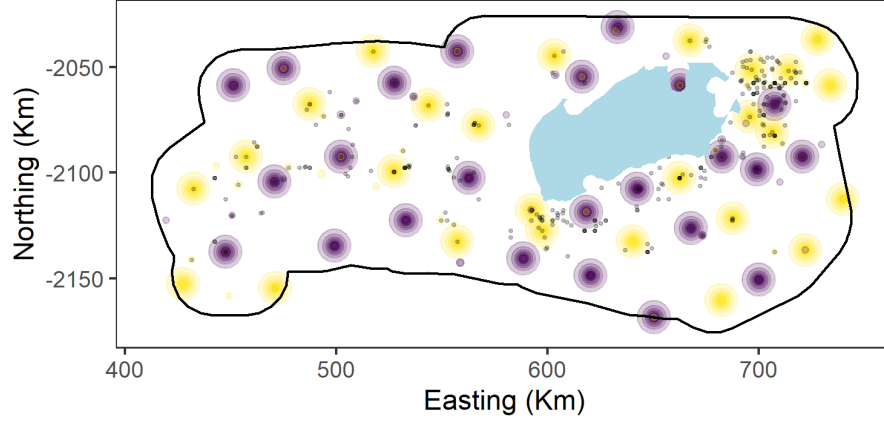


(a) Model Averaging

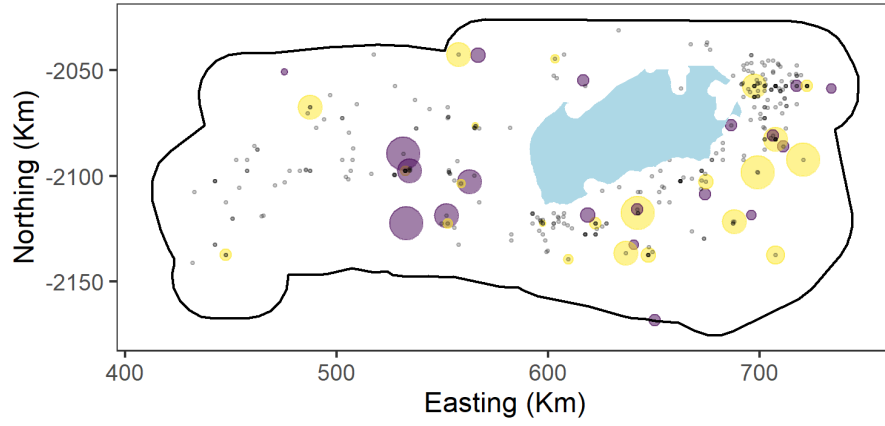


(b) SALSA 2D

**Figure 4.** Figure showing the intensity of carcass locations throughout the study area (ENP) using the model averaging (top) and SALSA2D (bottom). Note: to ensure detail can be seen, the two images have differing intensity scales. The carcass locations are shown as black circles. The blue polygon is the Etosha salt pan and the lines are the roads within the park.



(a) Model Averaging (11 models)



(b) SALSA 2D

**Figure 5.** Figure showing the knot locations and  $r$  from the best model averaging (top) and SALSA2D (bottom) models. Yellow is for a positive model coefficient and purple a negative one. The size of the coloured circles is a visual representation of the size of the  $r$  parameter. Note that in (a) the concentric rings are from models had the same knot locations with different  $r$ . In (b) the colours overlap but each  $k$  is in a different location. The carcass locations are shown as grey/black circles. The blue polygon is the Etosha salt pan.

## 427 5. Application: Analysis of Elephant mortality in Etosha National Park

### 428 5.1. Data available

429 The intensity of elephant carcasses, based on the observed carcass locations and  
430 pseudo-absences, was modelled using four candidate covariate terms: distance from  
431 the nearest road, distance from the nearest water point, mean annual rainfall and a  
432 spatial term based on spatial coordinates (in km, UTM zone 33S).

433 The distance from nearest road and nearest waterhole metrics were calculated using  
434 shape files supplied by the Ministry of Environment and Tourism (Namibia). These  
435 metrics were considered as candidates in the model to reflect possibly differential  
436 mortality rates near roads and waterholes, regardless of their spatial location in the  
437 park.

438 The mean annual rainfall was based on rainfall data collected from 168 rain gauges  
439 distributed across Etosha National Park which are visited annually, when possible.  
440 Annual rainfall was not available for every gauge for every year, due to logistical dif-  
441 ficulties reaching remote areas in some years, and so this metric was averaged across  
442 years for each gauge before interpolation to indicate areas in ENP with persistently  
443 high or low rainfall. The interpolation was achieved using a high dimensional pe-  
444 nalisised spline ( $df = 150$ ) to allow for interpolation to the carcass data locations and  
445 to the pseudo-absence grid. Details on the rainfall interpolation can be found in Sec-  
446 tion 4 of the supplementary material.

447 The proximity to waterholes was included as a candidate since elephant frequent wa-  
448 ter holes throughout the year, particularly in the dry season; roughly May to Octo-  
449 ber [14] and have been shown to have increased habitat use with proximity to water.  
450 [21].

451 While natural deaths might occur in line with their distributional patterns it is  
452 thought Anthrax-related deaths may be related to the use of water holes [22]. The  
453 relationship with waterholes was found to be very stepped and so this variable was  
454 converted to a 2 level factor;  $< 3\text{km}$  and  $\geq 3\text{km}$  (cutoffs of 1-5km were trialled and  
455 assessed using BIC).

456 The reasons for including proximity to roads as a candidate might seem less obvious,  
 457 but the attraction or repulsion to roads by elephants might also be evident in their  
 458 mortality patterns, and the model comparison work demonstrated that some roads  
 459 are important (Figure 4b). This could be due to elephant preference to be found  
 460 near roads, which is possible owing to their extensive use of roads/tracks for travel  
 461 [14], but can only be confirmed by a dedicated analysis of survey data or that the  
 462 detection of carcasses is higher near roads (e.g. easier to observe).  
 463 The spatial term was considered for inclusion in this model to represent the spatial  
 464 patterns in mortality that are not adequately explained by proximity to roads, water  
 465 holes or annual mean rainfall. The role of this term in this model is crucial in this  
 466 case - correctly identifying systematic spatial patterns in mortality might provide in-  
 467 sights about other park features not currently considered to be related to mortality  
 468 and overlooking these features prevents the mitigation of future elephant mortalities,  
 469 particularly those related to poaching.

## 470 **5.2. Model specification**

471 We are interested in modelling the intensity of elephant carcass locations as a func-  
 472 tion of distance to water, roads, mean annual rainfall and as a spatially adaptive  
 473 smooth function of spatial coordinates. The model specification was:

$$\begin{aligned}
 \log(\lambda(\mathbf{X}_i)) &= \eta_i \\
 &= \beta_0 + \text{distWater}_i + s_1(\text{rainfall}_i) \\
 &\quad + s_2(\text{distRoads}_i) + s_3(\mathbf{x}) \\
 &= \mathbf{X}_i^T \boldsymbol{\beta}
 \end{aligned}$$

474 In this case,  $\lambda(\mathbf{X}_i)$  is the intensity at location  $i$  and  $\mathbf{X}_i$  represents the coordinates  
 475 and environmental covariates.  $s_1$  and  $s_2$  represent one-dimensional basis functions,  
 476 while  $s_3(\mathbf{x})$  represents a two-dimensional exponential basis function for the spatial  
 477 coordinates.  $\boldsymbol{\beta}$  is a vector of model parameters associated with all columns of the

design matrix,  $\mathbf{X}$ . The columns of  $\mathbf{X}$  comprise the intercept (1), water  $\geq 3\text{km}$  (0,1),  $B$ -spline bases for rainfall and roads and the exponential radial basis for the spatial term.

Specifically, quadratic  $B$ -splines with SALSA based knot selection [5] were used to implement the one dimensional smooth terms for rainfall and roads. The two-dimensional spline basis function was determined using Equation 2 (exponential basis) and based on Euclidean distances. Knot number, their locations and  $r_k$  values were chosen using the SALSA2D algorithm. The starting parameters were based on the best result from the simulation study;  $k_s = 41$ ,  $k_{\min} = 2$  and  $k_{\max} = 100$ . The BIC was used to govern model selection in all cases.

### 5.3. Results

The results show that carcass intensity is highest near to water holes and roads (Figures 6 & 7) and locations where the annual rainfall is approximately 450mm (Figure 8). Specifically, intensity decreases steeply with the distance from road until approximately 1km when the relationship subsides.

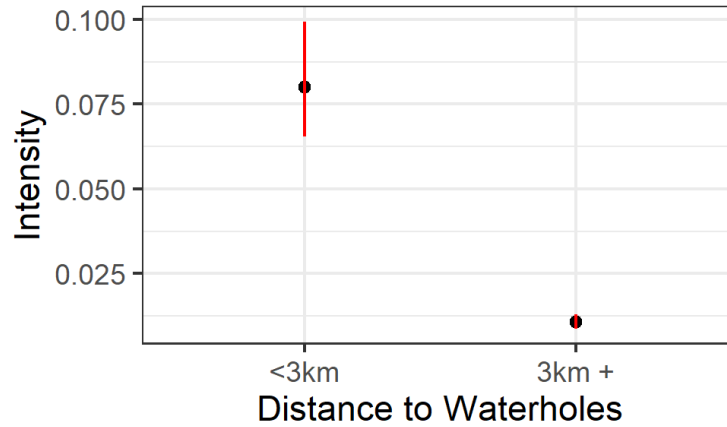


**Figure 6.** Figure showing the estimated relationship of distance to the nearest waterhole to carcass intensity (when distance to roads = 1.5km and mean annual rainfall = 420mm). The red line area is a 95% confidence interval about the estimated relationship.

The addition of distance from roads and mean annual rainfall to the spatial term, improved model results when compared with model results based on a SALSA2D-based spatial term alone (Models 2 and 3 Table 2); the BIC scores substantially im-

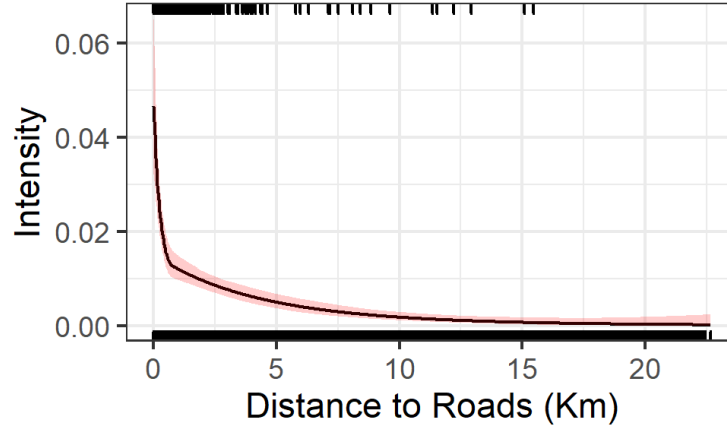


**Figure 7.** Figure showing the estimated relationship of distance to roads to carcass intensity (when mean annual rainfall = 420mm and distance to waterhole is  $\geq 3$ km). The red shaded area is a 95% confidence interval about the estimated relationship. The tick marks top and bottom show the values of the covariate in the original data which were presence locations (1's) and absences (0's).

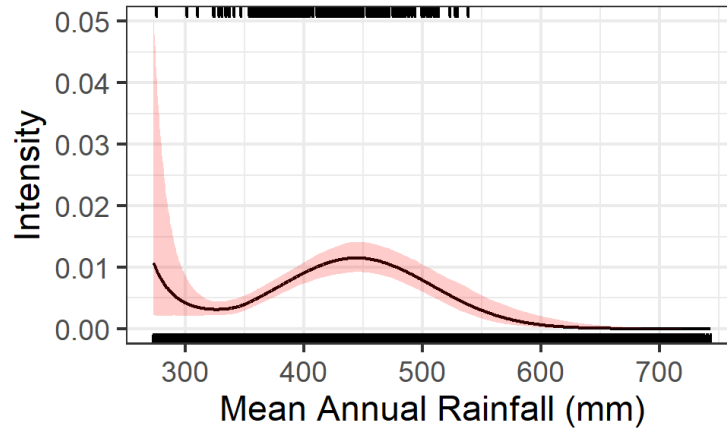


**Figure 8.** Figure showing the estimated relationship of mean annual rainfall to carcass intensity (when distance to road = 1.5km and distance to waterhole is  $\geq 3$ km). The red shaded area is a 95% confidence interval about the estimated relationship. The tick marks top and bottom show the values of the covariate in the original data which were presences (1's) and absences (0's).

496 proved from 2980 to 2848.

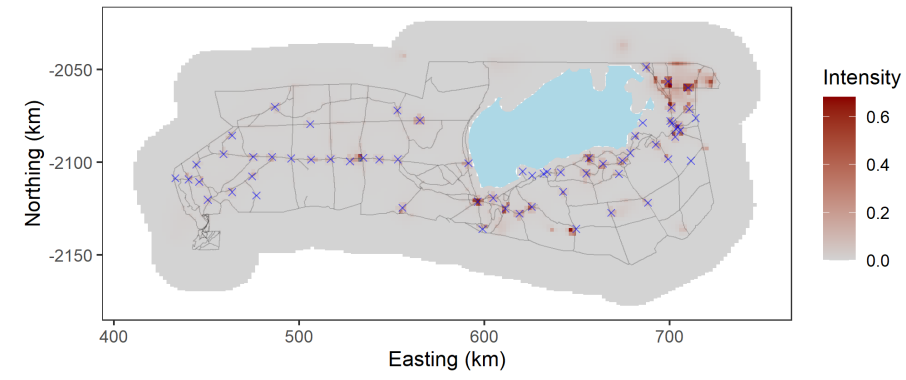
497 The spatial term also contributed positively to the model, despite the extra parame-  
 498 ters incurred (Table 2); the BIC score decreased from 3084 for the univariate model  
 499 (Model 1) to 2848 when the spatial term was included (Model 2). The practical con-  
 500 sequences of its inclusion was clearly evidenced by tempering the ‘global’ effect of  
 501 roads and water which was implicit in the model that included the additional vari-  
 502 ables (Figure 9a). In some cases the road and water effects diminished altogether  
 503 where carcasses were not seen in the data. Crucially, this spatial term also better



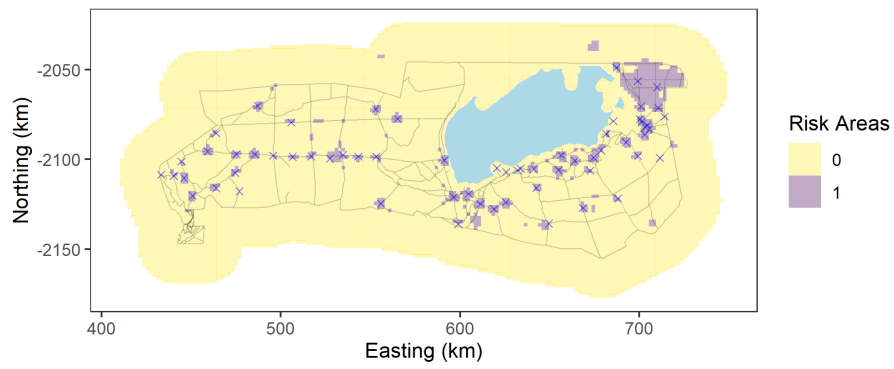
504 accommodates carcass locations which are not explained by only their proximity to  
505 water, distance to roads or average annual rainfall. Figure 10 shows that in Model  
506 1, the water hole relationship dominates with a peak of intensity at each one. When  
507 the spatial term is added, the waterhole peak is suppressed at a number of water-  
508 holes and even increased at others. The peak in intensity is shifted to the north  
509 which is in keeping with the high number of carcasses observed there. The knot lo-  
510 cations are similar to Model 3 but with fewer in the west and a higher proportion  
511 of smaller  $r$  (Figure 10b). Overall, the modelling shows that most, but not all, wa-  
512 terholes and some roads have high carcass intensity. Figure 9b shows the top 5%  
513 highest carcass intensity areas which form the highest risk areas in the park.

**Table 2.** Table showing the results for the model based on one dimensional smoother-based relationships only (model 1) and the model with both one and two dimensional smoothers (model 2). For reference, model 3 is the model with only a two dimensional smooth (see Table 1).

Model	Term	$df$	$\chi^2$ $p$ -value	Log-Likelihood	BIC
1	s(rainfall)	3	$p < 0.0001$	-1505.4	3084.4
	s(distRoads)	3	$p < 0.0001$		
	Near water	1	$p < 0.0001$		
2	s(rainfall)	3	$p < 0.0001$	-1221.3	2848.0
	s(distRoads)	3	$p < 0.0001$		
	Near water	1	$p < 0.0001$		
	s(xcoord, ycoord)	36	$p < 0.0001$		
3	s(xcoord, ycoord)	41	$p < 0.0001$	-1301.6	2980.1



(a)



(b)

**Figure 9.** Figure showing the estimated carcass intensity throughout the study area using SALSA and SALSA2D-based model selection and both one and two dimensional spline based terms (a). Figure showing the top 5% intensity areas. The carcass locations are shown as black circles, the blue polygon is the Etosha salt pan, the blue crosses are waterholes and the black lines are roads.

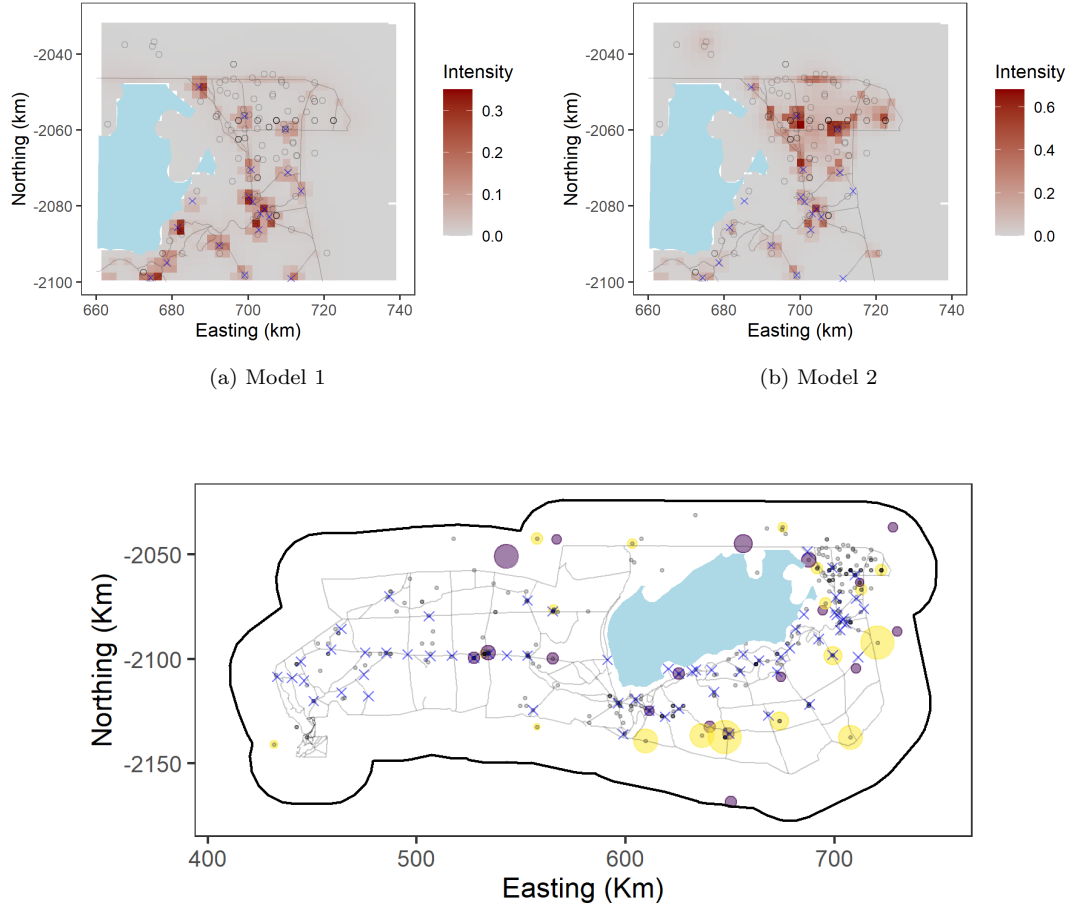


**Figure 10.** Figure showing the estimated carcass intensity for the north east part of the study area for (a) Model 1, (b) Model 2 and (c) the location of  $k$  and associated  $r$  for model 2. The carcass locations are shown as black circles, the blue polygon is the Etosha salt pan, the blue crosses are waterholes and the black lines are roads

## 514 6. Discussion

515 Using SALSA2D for model selection provided better results and the ability to have  
516 a more realistic local/clustered intensity surface compared with the model averag-  
517 ing approach. There are clear numerical and practical benefits to SALSA2D-based  
518 model selection compared with a model averaging approach in this case and while  
519 the benefits of doing so might be less stark in cases where spatial patterns are more  
520 smooth, it needs to be possible to identify clusters and irregular patterns, such as  
521 those observed here, when they exist.

522 Simply including proximity to water and roads in the model as part of this  
523 analysis did not reveal genuine patterns in all areas of the park, since not all  
524 roads/waterholes have been associated with carcasses. The addition of the spatial  
525 term with spatially adaptive knot selection was able to suppress/enhance the global  
526 relationships with the environmental covariates in particular areas. This resulted in  
527 the identification of some critical areas of the park which is important for effective  
528 park management, both in terms of disease outbreak, which after ‘unknown’ was the  
529 largest category, and poaching, which although small in this data set ( $<1\%$  of car-  
530 casses), occurs in the park. It is impossible to patrol such a large area at random  
531 and the areas of the park identified here (particularly those accessed by a subset of  
532 roads/waterholes) appear to require more monitoring efforts than others. Elephants  
533 are highly mobile and so early detection of carcasses, in particular anthrax related  
534 deaths, are important to identify spread of disease across the park [23].

535 This extended CReSS approach using SALSA2D model selection is of immedi-  
536 ate and practical value to a wide range of users of statistical modelling methods.  
537 SALSA2D is implemented inside the `MRSea` package and it can automatically select  
538 knots based on two user-defined types of two-dimensional spline bases (Gaussian  
539 and exponential) and distance calculation (Euclidean or geodesic) based on a range  
540 of objective fitness criteria, chosen by the user. Notably, exclusion zones and non-  
541 Euclidean distances can be included to model more complex spatial regions [as seen  
542 in 4, 6] and adaptations have been made to allow for the fitting of Poisson PPMs  
543 using the downweighted Poisson regression method. By using presence only data in

544 this paper, as opposed to the more traditional Binomial or Poisson GAMs, we have  
545 demonstrated the flexibility of this approach for a wide variety of settings.

## 546 **7. Supplementary Material**

547 See additional document for information on residual calculation, pseudo-absence se-  
548 lection, expanded results of the methods comparison and details of rainfall interpola-  
549 tion.

### 550 ***Acknowledgements***

551 The authors would like to thank Dr. Richard Glennie for his assistance and patience  
552 with PPM queries and reading a draft of the paper.

### 553 ***Notes on contributors***

- 554 • LSH, MLM and CGW contributed to method development, analysis and pa-  
555 per writing
- 556 • GS, WK and PdP contributed to data collection and local information

### 557 ***Disclosure Statement***

558 There are no competing interests.

### 559 ***Funding***

560 The authors declared that no grants were involved in supporting this work.

## 561 **References**

- 562 [1] MIKE. <https://cites.org/eng/prog/mike>, 2018. URL [https://cites.org/eng/prog/](https://cites.org/eng/prog/mike)  
563 [mike](https://cites.org/eng/prog/mike).
- 564 [2] W. C. Turner, P. Imologhome, Z. Havarua, G. P. Kaaya, J. K. E. Mfunu, I. D. T.

- 565 Mpofu, and W. M. Getz. Soil ingestion, nutrition and the seasonality of anthrax in  
566 herbivores of Etosha National Park. *Ecosphere*, 4(1):13, 2013. .
- 567 [3] T. Karombo. Elephants are dying in droves in botswana. scientists  
568 don't know why, 2021. URL [https://www.sciencenews.org/article/](https://www.sciencenews.org/article/african-elephant-mass-death-botswana)  
569 [african-elephant-mass-death-botswana](https://www.sciencenews.org/article/african-elephant-mass-death-botswana).
- 570 [4] L. A. S. Scott-Hayward, M. L. Mackenzie, C. R. Donovan, C. G. Walker, and E. Ashe.  
571 Complex Region Spatial Smoother (CReSS). *Journal of Computational and Graphical*  
572 *Statistics*, 23(2):340–360, 2014.
- 573 [5] C.G. Walker, M.L. Mackenzie, C.R. Donovan, and M.J. O'Sullivan. SALSA - a  
574 Spatially Adaptive Local Smoothing Algorithm. *Journal of Statistical Computation*  
575 *and Simulation*, 81(2):179–191, 2010.
- 576 [6] L.A.S. Scott-Hayward, Mackenzie M.L., and C.G. Walker. MRSea package: Statistical  
577 modelling of bird and cetacean distributions in offshore renewables development areas,  
578 2021.
- 579 [7] R Core Team. *R: A Language and Environment for Statistical Computing*. R Founda-  
580 tion for Statistical Computing, Vienna, Austria, 2019. URL [https://www.R-project.](https://www.R-project.org/)  
581 [org/](https://www.R-project.org/).
- 582 [8] M.E. Johnson, L.M. Moore, and D. Ylvisaker. Minimax and maximin distance designs.  
583 *Journal of Statistical Planning and Inference*, 26:131–148, 1990.
- 584 [9] D. J. F. Russell, G. D. Hastie, D. Thompson, V. M. Janik, P. S. Hammond, L. A. S.  
585 Scott-Hayward, J. Matthiopoulos, E. L. Jones, and B. J. McConnell. Avoidance of wind  
586 farms by harbour seals is limited to pile driving activities. *Journal of Applied Ecology*,  
587 53(6):1642–1652, 2016.
- 588 [10] R. A. Dunlop, M. J. Noad, R. D. McCauley, L. Scott-Hayward, E. Kniest, R. Slade,  
589 D. Paton, and D. H. Cato. Determining the behavioural dose–response relationship  
590 of marine mammals to air gun noise and source proximity. *Journal of Experimental*  
591 *Biology*, 220(16):2878–2886, 2017.
- 592 [11] D. V. Harris, J. L. Miksis-Olds, J. A. Vernon, and L. Thomas. Fin whale density and  
593 distribution estimation using acoustic bearings derived from sparse arrays. *The Journal*  
594 *of the Acoustical Society of America*, 143(5):2980–2993, 2018.
- 595 [12] Nariaki S. Further analysts of the data by Akaike's information criterion and the finite  
596 corrections. *Communications in Statistics - Theory and Methods*, 7(1):13–26, 1978.
- 597 [13] C. F. Dormann, J. M. Calabrese, G. Guillera-Arroita, E. Matechou, V. Bahn,

598 K. Bartoń, C. M. Beale, S. Ciuti, J. Elith, K. Gerstner, et al. Model averaging in ecol-  
599 ogy: a review of bayesian, information-theoretic, and tactical approaches for predictive  
600 inference. *Ecological Monographs*, 2018.

601 [14] M. Tsalyuk, W. Kilian, B. Reineking, and W. M. Getz. Temporal variation in resource  
602 selection of African elephants follows long-term variability in resource availability. *Eco-  
603 logical Monographs*, 89(2):e01348, 2019. .

604 [15] D. I. Warton and L. C. Shepherd. Poisson point process models solve the “pseudo-  
605 absence problem” for presence-only data in ecology. *The Annals of Applied Statistics*, 4  
606 (3):1383 – 1402, 2010. .

607 [16] I. W. Renner and D. I. Warton. Equivalence of MAXENT and poisson point process  
608 models for species distribution modeling in ecology. *Biometrics*, 69(1):274–281, 2013. .

609 [17] M. Berman and T. R. Turner. Approximating point process likelihoods with GLIM.  
610 *Journal of the Royal Statistical Society. Series C (Applied Statistics)*, 41(1):31–38,  
611 1992.

612 [18] N. Cressie. *Statistics for spatial data*. John Wiley & Sons, New York, 1993.

613 [19] R. W. Floyd. Algorithm 97: Shortest path. *Communications of the ACM*, 5:345, 1962.

614 [20] G. Schwarz. Estimating the dimension of a model. *Ann. Statist.*, 6(2):461–464, 03 1978.  
615 .

616 [21] G. M. Harris, G. J. Russell, R. I. van Arde, and S. L. Pimm. Rules of habitat use by  
617 elephants *Loxodonta africana* in southern Africa:in sights for regional management.  
618 *Oryx*, 41(42 (1)):66–75, 1992.

619 [22] R. Zidon, S. Garti, W. M. Getz, and D. Saltz. Zebra migration strategies and anthrax  
620 in Etosha National Park, Namibia. *Ecosphere*, 8(8):e01925, 2017. .

621 [23] P. Lindeque and P. C. B. Turnbull. Ecology and epidemiology of anthrax in the Etosha  
622 National Park, Namibia. *The Onderstepoort Journal of Veterinary Research*, 61 1:71–  
623 83, 1994.